Published in final edited form as:
Retina. 2013 January ; 33(1): 232–236. doi:10.1097/IAE.0b013e31826e86f5.

Visualization of Real-Time Intraoperative Maneuvers with a Microscope-Mounted Spectral Domain Optical Coherence Tomography System

Justis P. Ehlers, MD[*,†], **Yuankai K. Tao, PhD**[‡], **Sina Farsiu, PhD**[†], **Ramiro Maldonado, MD**[†], **Joseph A. Izatt, PhD**[†,‡], and **Cynthia A. Toth, MD**[†,‡]

[*]Vitreoretinal Service, Cole Eye Institute, Cleveland Clinic Foundation, Cleveland, Ohio

[†]Vitreoretinal Service, Duke Eye Center, Duke University Medical Center, Durham, North Carolina

[‡]Department of Biomedical Engineering, Duke University, Durham, North Carolina

Keywords

optical coherence tomography; retinal surgery; microscope OCT; MMOCT; *i*OCT; image-guided surgery

The advent of optical coherence tomography (OCT) has revolutionized our diagnostic and therapeutic capabilities in ophthalmology and vitreoretinal disease. In the clinic setting, OCT has touched nearly every aspect of vitreoretinal disease. More recently, OCT has been introduced the operating room theater. Intraoperative OCT (*i*OCT) has been used to successfully further our understanding of optic pit maculopathy, macular holes, epiretinal membranes, and retinopathy of prematurity.[1–6] Limited systems are available for intraoperative use. All commercially available systems are handheld OCT devices or modified tabletop units, which allow for intraoperative imaging but require cessation of the surgical procedure to complete imaging. This precludes real-time feedback to the surgeon of the anatomical impact of surgical maneuvers and increases the duration of the surgical procedure. A microscope-mounted/integrated OCT (MMOCT) system allows for the integration of OCT into the real-time surgical platform.[7,8] At the time of this report, two unique prototype systems have been described in the literature.[5,7,8] Using a prototype MMOCT system, we previously demonstrated the feasibility of intraoperative imaging of surgical instruments, retinal effects of surgical contact, and primarily static surgical steps.[7] To further seamlessly integrate OCT into the surgical platform, visualization of intraoperative motion and manipulation will be critical. Another critical component of integration will include the rapid localization of the surgical area of interest with the

Reprint requests: Cynthia A. Toth, MD, Box 3802, Duke University Medical Center, Durham, NC 27710; cynthia.toth@duke.edu.

Consultant: Alcon and Genentech (C.A.T.); intellectual property rights: Bioptigen (C.A.T., Y.K.T., J.A.I.) and Alcon (C.A.T.); ownership interest: Bioptigen (J.A.I., Duke University); patent application: system enhancements for ophthalmic surgical microscope-mounted optical coherence tomography (J.A.I., C.A.T., Y.K.T., J.P.E.).

Supplemental digital content is available for this article. Direct URL citations appear in the printed text and are provided in the HTML and PDF versions of this article on the journal's Web site (www.retinajournal.com).

intraoperative spectral domain OCT (SD-OCT) device and quantitative information regarding the relative locations of the surgical instruments to the retinal tissue layers of interest. In this report, we describe a novel technique for visualizing intraoperative motion of surgical instruments with an MMOCT system.

Methods

Prototype OCT Design

An MMOCT was developed to fit a Leica (Wetzlar, Germany) operating microscope while using the optical path of the Oculus (Wetzlar, Germany) BIOM3, as previously described.[7,8] Critical to the design of the microscope was to give an unaltered view to the surgeon through the operating microscope. The prototype scan rate is 20,000 A-scans per second. Given that speed, the MMOCT is capable of capturing 78 B-scans per second, with each comprising of 256 A-scans. At this resolution, we can detect all retinal layers at 5 neighboring azimuthal positions at 16 frames per second.

Intraoperative Simulation with Model Eyes

Fresh cadaveric porcine eyes were obtained for imaging, and OCT scanning was performed within 12 hours of harvest to optimize corneal clarity. A suction plate was used to fixate the eye, and the surgical microscope and MMOCT was positioned over the eye. A 19-g microvitreoretinal (MVR) blade was used to create 2 sclerotomies. A fiber optic light was used for illumination, and the instrument of interest was placed through the second sclerotomy. The BIOM was used to adjust the coincident focus for both the surgeon and MMOCT.

Intraoperative Imaging Protocol

Multiple scan methods were evaluated to follow instrument motion and view the instrument–tissue interaction during a maneuver. Using the MMOCT device to obtain the scans, Bioptigen v1.6 (Bioptigen, Research Triangle Park, NC) was used to operate the device, test the scan protocols, and acquire the raw data from the scans. Image averaging, registration, and postprocessing were performed using ImageJ (freeware; National Institutes of Health, Bethesda, MD) and Matlab 2010a (Matlab; MathWorks, Natick, MA). In addition to a traditional scan protocol (e.g., 15 × 15 mm with 500 B-scans by 500 A-scans), multiple variations of scan protocols were tested to achieve the capture of dynamic imaging. Tested protocols included B-scans parallel and perpendicular to the instrument tip, large and small sampling areas, and variations of scan dimensions (e.g., square, rectangular). Additionally, scans were assessed both with and without averaging over the scanned area for optimal visualization of intraoperative motion.

Instruments

The metallic 36-gauge beveled retinal needle (Alcon, Fort Worth, TX) and the diamond-dusted membrane scraper (Synergetics, O’Fallon, MO) were selected for use in this study. These instruments were selected based on the OCT characteristics of the instruments allowing for a variation in instrument sizes, types of surgical manipulations, reflectivity profiles, and shadowing characteristics.[7]

Results

Optimized Scan Protocol

Traditional scan protocols (e.g., 15 × 15 mm with 500 B-scans by 500 A-scans) did not allow for imaging of intraocular motion. First, because of the large area scanned and the time required to complete the scan, instrument motion occurred while scanning progressed outside the view of the instrument. Second, because of the shadowing from the instrument, it was difficult to assess the relationship to the underlying retinal tissue. To customize the device scan protocol for intraoperative motion, several methods of rapid refresh rates of scanning over a small area were developed and tested on the surgical instrument of interest. From various scan lengths and angles relative to the instrument, the following scan method was found to be optimal for visualizing instrument motion. The surgical maneuver scanning protocol captured 5 B-scans, comprising of 256 A-scans each along the axis of the instrument, over an 8.0 mm × 0.4 mm field of view. The scans were oriented such that the densely sampled long scanning axis (i.e., 8.0 mm) was aligned (i.e., parallel) along the axis of the instrument. This axis was also parallel to the direction of the motion associated with the surgical maneuver. The B-scans showed regions of tissue deformation and discrete portions of the surgical instrument that incidentally overlapped with the MMOCT interrogation beam. To optimize the visualization of instrument–tissue interactions, the series of B-scans obtained over the short scan axis (0.4 mm) were coregistered and averaged to create a pseudo real-time image of instrument dynamics. This ensured that instrument cross sections were captured in every frame despite instrument motion, which is of particular importance when imaging thin devices (e.g., retinal needle cross sections) in the setting of subtle oscillations of surgical motion. In addition, this provided both underlying retinal information and the location of the surgical instrument in the same summed frame, eliminating most of the confusion from shadowing.

Intraoperative Maneuver Imaging

The diamond-dusted membrane scraper and retinal needle were successfully imaged on the summed voxel projection (SVP), B-scan, and with three-dimensional rendering. The scraper had a high reflectivity profile because of the diamond dusting (Figure 1A). Increased shadowing compared to the more proximal bare silicone was noted in the area of the diamond coating. The shadowing was not absolute, and the underlying tissues could still be visualized. Averaging of B-scans over the total area of the scan provided improved image quality and decreased the loss of retinal revisualization from shadowing (Figure 1B). Dynamic imaging of the intraoperative motion was successfully obtained while engaging the retinal surface with membrane scraper. Linear passes with the membrane scraper were well visualized on B-scans (Figure 2, see Video 1, Supplemental Digital Content 1, http://links.lww.com/IAE/A114).

The retinal needle showed absolute shadowing with bright reflectivity at the edge of the instrument (Figure 3A). Averaging of scans over the area of the retinal needle provided improved image quality and significantly improved the underlying shadowing (Figure 3B). The retinal needle was used to engage the retinal tissue and apply anterior traction on the retinal tissue. The interactions between the retinal needle and retinal tissue were successfully

visualized (Figure 4, see Video 2, Supplemental Digital Content 1, http://links.lww.com/IAE/A115).

For both the diamond-dusted membrane scraper and the retinal needle, summation of the B-scans during dynamic imaging over the area of scanning allowed for improved visualization of the instrument due to compensation for slight deviations off the scan axis during instrument movement. Additionally, the summation decreased the impact of the shadowing of the instrument by including images of the retina without shadowing from the tissue immediately adjacent to the site of the shadow.

During dynamic imaging of intraoperative motion, several limitations were identified. To visualize intraoperative motion, instrumentation either with partial shadowing and high scattering properties (i.e., diamond-dusted membrane scraper) or with small areas of shadowing (i.e., retinal needle) was required. This limited the types of instruments that could be tested. The area of scanning was also reduced to focus on a width that was approximately the same as the instrument of interest. Because of the reduced area of scanning, the surgeon was required to move only along the scan axis to maintain visualization of the instrument. However, the reduced area of scanning was necessary to provide a rapid scanning loop for the area of interest that allowed for imaging of motion. The lack of active targeting to the instrument tip by the OCT device required significant coordination between the surgeon and the individual running the OCT device. Alignment of the instrument and the scan area was required to appropriately visualize the instrument. Any deviation from the scan area resulted in loss of instrument visualization from the OCT scan.

Discussion

The use of *i*OCT has advanced our understanding of the impact of surgical maneuvers on various disease states. Portable cart systems with a handheld SDOCT imaging head have allowed for this intraoperative use. Multiple conditions have been described with *i*OCT. Changes in macular hole configuration, ultrastructural alterations after removal of epiretinal membrane, the impact of aspiration over the optic pit in optic pit maculopathy, and novel features of retinopathy of prematurity have all been described with *i*OCT.[1–3,5,6] However, real-time analysis of intraoperative maneuvers is not feasible without an integrated system.

In this report, we describe a novel method of visualizing intraoperative motion and maneuvers using an MMOCT system in a model eye. Dynamic imaging of intraoperative motion with SDOCT poses several challenges. Using a microscope-mounted system addresses the issue of halting the surgical procedure to obtain images. However, the cross-sectional nature of the B-scan and the static nature of the OCT images provide significant obstacles to imaging intraoperative motion. The typical scan used for clinical OCT is a large square area (e.g., 10 × 10 mm). This type of scan does not allow for efficient and satisfactory capture of intraocular motion. The instrument and area of interest occupy only a small width of the typical scan (e.g., 0.4 mm). Any movement of the instrument is missed while the rest of the scan is completed. Using this type of scan, only static images of instrument–tissue interaction can be obtained. To address the static nature of the captured images, the length of the axis perpendicular to the instrument axis was reduced to allow for a

rapid looped scan sequence and to focus the field of view on the instrument of interest. Averaging sequential B-scans with spatial compounding removed any positional ambiguity between the MMOCT interrogation beam and instrument, allowed for improved visualization of the instrument–tissue interactions, and significantly reduced shadowing artifacts below the instrument.

Several limitations continue to exist for real-time viewing of intraoperative motion. For future use, real-time simultaneous image processing will need to be implemented to provide optimal and efficient image feedback to the surgeon. Because of the small scanning area and lack of targeting to the instrument tip, significant coordination was necessary between the individual running the scanner and the surgeon. Additionally, linear surgical maneuvers were required to maintain constant visualization. Targeting of the OCT scanner to the area of interest will be necessary to achieve rapid image acquisition and to allow for maneuvers on all axes.

Recent advances in image processing may be used to develop an adaptive framework for real-time MMOCT imaging and analysis with applications in vitreoretinal surgery, including identification of instruments and the surgical area of interest. Current generation SDOCT systems, as fast as they are compared with time-domain technology, still cannot perform three-dimensional retinal imaging at a sufficient rate to be useful to the surgeon for real-time feedback. It is also not clear whether three-dimensional reconstruction compared with two-dimensional B-scans would be advantageous to the surgeon. Using real-time image processing from two noninvasive imaging devices, complementary synchronized information can be obtained, such as from a spectrally encoded confocal scanning laser ophthalmoscope integrated with an SDOCT system.[9] The spectrally encoded confocal scanning laser ophthalmoscope allows for fundus images to be obtained as a data source for aiming and registration of the OCT beam. The fundus images give rough estimates of the surgical instrument’s position within the eye, allowing correlation with the appropriate SDOCT location.

Image processing may be used to provide a key component of the integration of OCT into real-time operative use: targeting of the OCT scanner to the area of interest. Two particular techniques can be used to track small displacements of the instruments through a Kalman filtering technique as well as the large movements from the surgeon’s hands by identifying the curvilinear tools on the spectrally encoded confocal scanning laser ophthalmoscope images.[10,11] Advanced image processing may also provide techniques for relaying quantitative depth information regarding the instrument and its relationship to the retinal tissues of interest, such as automated segmentation.[12] Using automated real-time segmentation of the OCT scan, quantitative measurements of the distance between the instrument and various retinal layers could be relayed to the surgeon in real time. The distance from the tip of the surgical tool to retinal layers could be relayed to the surgeon through various mechanisms (e.g., audio proximity alarms, visual depth guides).

In this report, intraoperative motion is successfully captured using a prototype MMOCT system. This advancement in *i*OCT techniques will provide a foundation for future research in intraoperative integration of OCT. Important future directions of research include

adaptation of image processing to include the analysis of the instrumentation, real-time surgical instrument–tissue proximity information, development of efficient protocols for targeting the OCT scan device to the area of interest, and translation of intraoperative imaging to human subjects.

Supplementary Material

Refer to Web version on PubMed Central for supplementary material.

Acknowledgments

Research was funded in part by NCRR 1UL1 RR024128-01 and NEI R21-EY-019411.

References

1. Ehlers JP, Kernstine K, Farsiu S, et al. Analysis of pars plana vitrectomy for optic pit-related maculopathy with intraoperative optical coherence tomography: a possible connection with the vitreous cavity. Arch Ophthalmol. 2011; 129:1483–1486. [PubMed: 22084218]
2. Chavala SH, Farsiu S, Maldonado R, et al. Insights into advanced retinopathy of prematurity using handheld spectral domain optical coherence tomography imaging. Ophthalmology. 2009; 116:2448–2456. [PubMed: 19766317]
3. Dayani PN, Maldonado R, Farsiu S, Toth CA. Intraoperative use of handheld spectral domain optical coherence tomography imaging in macular surgery. Retina. 2009; 29:1457–1468. [PubMed: 19823107]
4. Scott AW, Farsiu S, Enyedi LB, et al. Imaging the infant retina with a hand-held spectral-domain optical coherence tomography device. Am J Ophthalmol. 2009; 147:364–373. e2. [PubMed: 18848317]
5. Binder S, Falkner-Radler CI, Hauger C, et al. Feasibility of intrasurgical spectral-domain optical coherence tomography. Retina. 2011; 31:1332–1336. [PubMed: 21273942]
6. Ray R, Baranano DE, Fortun JA, et al. Intraoperative microscope-mounted spectral domain optical coherence tomography for evaluation of retinal Anatomy during macular surgery. Ophthalmology. 2011; 118:2212–2217. [PubMed: 21906815]
7. Ehlers JP, Tao YK, Farsiu S, et al. Integration of a spectral domain optical coherence tomography system into a surgical microscope for intraoperative imaging. Invest Ophthalmol Vis Sci. 2011; 52:3153–3159. [PubMed: 21282565]
8. Tao Y, Ehlers J, Toth C, Izatt J. Intraoperative spectral domain optical coherence tomography for vitreoretinal surgery. Opt Lett. 2010; 35:3315–3317. [PubMed: 20967051]
9. Tao Y, Farsiu S, Izatt J. Interlaced spectrally encoded confocal scanning laser ophthalmoscopy and spectral domain optical coherence tomography. Biomed Opt Express. 2010; 1:431–440. [PubMed: 21258478]
10. Peterfreund N. Robust tracking of position and Velocity with Kalman Snakes. IEEE Trans Pattern Anal Mach Intell. 1999; 21:564–569.
11. Ulrich M, Steger C, Baumgartner A. Real-time object recognition using a modified generalized Hough transform. Pattern Recogn. 2003; 36:2557–2570.
12. Chiu S, Li X, Nicholas P, et al. Automatic segmentation of seven retinal layers in SDOCT images congruent with expert manual segmentation. Opt Express. 2010; 18:19413–19428. [PubMed: 20940837]

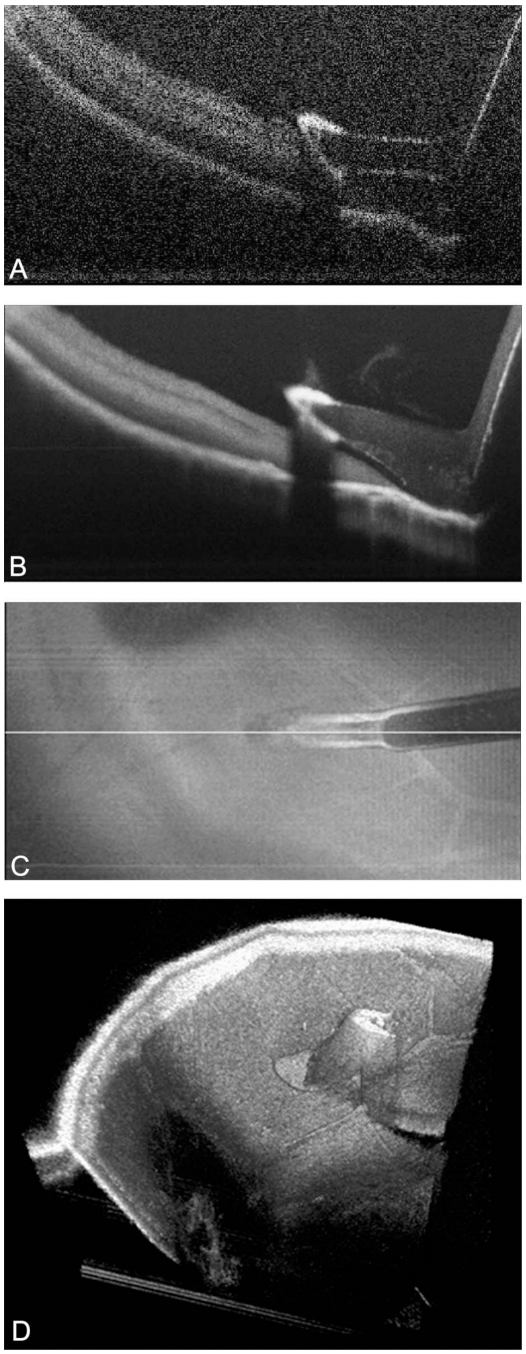

Fig. 1.

Microscope-mounted OCT image of diamond-dusted membrane scraper with cadaveric porcine retina. Image shows typical cadaveric porcine retina characteristics with high reflectance and minimal layering within retinal architecture. **A.** Single B-scan of diamond-dusted membrane scraper showing increased reflectance at area of diamond coating with increased shadowing. **B.** Summed B-scan series of diamond-dusted membrane scraper with improved tissue and instrument visualization and decreased shadowing under the silicone sleeve. Significant shadowing persists under the diamond coating. **C.** Summed voxel

projection of diamond-dusted membrane scraper on retinal surface. **D.** Three-dimensional reconstruction of diamond-dusted membrane scraper on retinal surface.

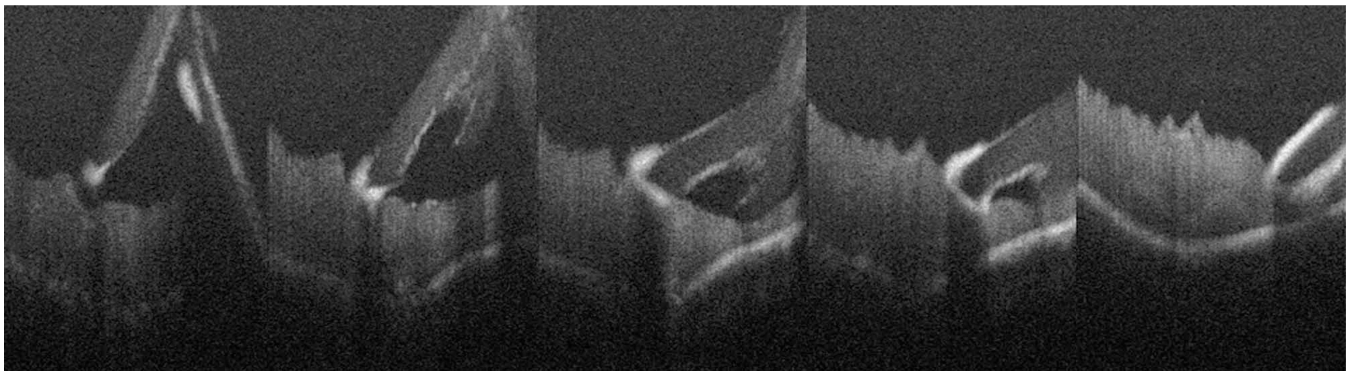

Fig. 2.

Microscope-mounted OCT capture of intraocular maneuvers with diamond-dusted membrane scraper with cadaveric porcine retina. Individual frames of B-scans selected from video capture of intraocular motion. Lateral and vertical motions of the diamond-dusted membrane scraper visualized (refer to Video 1, Supplemental Digital Content 1, http://links.lww.com/IAE/A114 for full sequence).

Fig. 3.

Microscope-mounted OCT image of 36-gauge retinal needle with cadaveric porcine retina. **A.** Single B-scan of retinal needle showing high reflectance at area of needle with absolute shadowing of underlying tissue. **B.** Summed B-scan series of retinal needle showing improved tissue visualization and significant improvement in shadowing. **C.** Summed voxel projection of retinal needle on retinal surface.

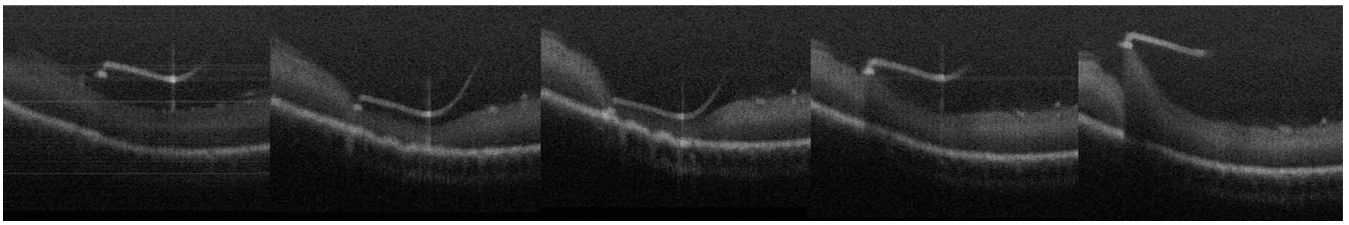

Fig. 4.

Microscope-mounted OCT capture of intraocular maneuvers with retinal needle with cadaveric porcine retina. Individual frames of B-scans selected from video capture of intraocular motion. Lateral and vertical motions of the retinal needle visualized with visible effects of traction applied to retinal surface (refer to Video 2, Supplemental Digital Content 1, http://links.lww.com/IAE/A115 for full sequence).